Nanomolar Binding of an Antibiotic Peptide to DNA Measured with Raman Spectroscopy

Grant J. Myres and Joel M. Harris*
Department of Chemistry, University of Utah, 315 South 1400 East
Salt Lake City, UT 84112-0850 USA

Abstract

Immobilization of DNA to surfaces offers a convenient means of screening the binding affinity and selectivity of potential small-molecule therapeutic candidates. Unfortunately, most surface-sensitive methods for detecting these binding interactions are not informative of molecular structure, information that is valuable for understanding the non-covalent interactions that stabilize binding. In this work, we report a method to meet this challenge by employing confocal Raman microscopy to quantify the association of a minor-groove-binding antimicrobial peptide, netropsin, to duplex-DNA hairpin sequences immobilized on the interior surfaces of porous silica particles. To assess binding selectivity, particles functionalized with different sequences of DNA were equilibrated with solutions of 100-nM netropsin, and selective association was detected based on the presence of netropsin Raman scattering in the particles. The selectivity study revealed that netropsin binds to sequences of duplex-DNA having AT-rich recognition regions. To quantify binding affinities, these AT-rich DNA sequences were equilibrated with a range of netropsin solution concentrations (1 to 100 nM). Raman scattering intensities of netropsin versus solution concentration were well described by single-binding-site Langmuir isotherms with nanomolar dissociation constants, in agreement with previous isothermal calorimetry and surface-plasmon resonance results. Target sequence binding was accompanied with changes in netropsin and DNA vibrational modes consistent with the hydrogen bonding between the amide groups of netropsin and adenine and thymine bases in the DNA minor groove. The binding of netropsin to a control sequence lacking the AT-rich recognition region exhibited an affinity nearly 4-orders-of-magnitude weaker than found for the target sequences. The Raman spectrum of netropsin interacting with this control sequence showed broad pyrrole and amide mode vibrations at frequencies similar to free solution, revealing a less constrained conformations compared with the specific binding interactions observed with AT-rich sequences.

*Corresponding author: harrisj@chem.utah.edu

INTRODUCTION

Small molecules that target specific sequences or structures of DNA have direct applications related to in-vivo sensing in cells,[1-4] modulation of gene expression,[5, 6] and cancer therapies.[7-9] Crucial to the discovery, development, and applications of small molecules that bind to DNA is quantitative measurement of their association affinity toward respective recognition sequences. Surface-based assays are especially well suited to this task, where a small population of surface-immobilized DNA can be reacted with molecules that bind with high affinity from small volumes of nanomolar solutions. Based on these requirements, surface-plasmon resonance (SPR) has emerged as a valuable label-free surface-assay for screening and measuring both affinities and kinetics of small-molecule association with surface-immobilized DNA.[10, 11]

Despite the attractive attributes of SPR for this application, SPR is unable to provide insight into the structure and conformations of the surface-localized molecules. This information is key to understanding the intermolecular interactions that are responsible for the association between sequences of DNA and small molecules. Raman spectroscopy is potentially well suited for characterization of biomolecular recognition; the method is label-free, quantitative, and structurally informative, and water produces little background in the fingerprint region of the vibrational spectrum. Previous applications of Raman spectroscopy have included characterization of DNA secondary structure,[12-15] discerning between differences in DNA duplex primary sequence,[16, 17] along with characterizing modulations of DNA structure, induced through non-covalent interactions with small molecules[18, 19]. Because Raman scattering cross sections are small ($\sim 10^{-28}$ cm^2), the small number of biomolecules immobilized in a monolayer on a planar surface are extremely challenging to detect. As a result, applications of Raman spectroscopy to investigate DNA/small-molecule interactions have been limited to solution-phase measurements with high concentrations of both DNA and the corresponding small molecule.

To address the challenge of applying Raman spectroscopy to study surface-localized DNA, we have recently developed a methodology that employs confocal Raman microscopy to characterize DNA immobilized on the internal surfaces of individual porous silica particles.[20] In contrast to conventional 2-dimenional planar substrates where detecting molecules at a surface is limited to the area of the excitation laser beam, DNA immobilized on the surfaces of nanoporous silica occupy a 3-dimensional volume. When this internal surface within an individual porous particle is probed by confocal Raman microscopy, the volume probed contains a ~1,500-fold greater surface area compared to a planar surface.[20] With this approach, the local internal concentration of immobilized DNA within a porous silica particle can be as high as ~30 mM, allowing label-free DNA detection by unenhanced, spontaneous Raman scattering.[20] This concept

has been applied in a hybridization assay capable of quantifying differences in the length and base content of target strands that are captured from solution by a probe sequence immobilized on porous silica surfaces. The hybridization of two target strands of equivalent length but different sequences can also be distinguished, along with a single-nucleotide polymorphism compared to a fully-complementary strand. These differences in structure are resolved based on detectable differences in respective intensities of base-specific vibrational modes. [20]

In the present work, we apply this method to determine the association selectivity, affinity, and interactions of a small molecule, netropsin, with different surface-immobilized DNA hairpin sequences. Netropsin is a natural product that was among the first small molecules observed to form strong and selective associations (K_d ~ 3–25 nM) with the minor groove of specific AT-rich sequences of duplex-DNA.[21-23] The AT-rich sequences that produce high-affinity interactions with netropsin can be used to assess the selectivity of the Raman spectroscopy measurement, by equilibrating netropsin with immobilized DNA that has or lacks these specific sequences. As a benefit compared to SPR screening, Raman spectra can reveal the nature of the binding interactions between the immobilized DNA and netropsin from frequency shifts and intensity changes in their respective vibrational modes. In addition to screening small molecule binding selectivity, the affinity of active sequences can be assessed by performing assays over a range of netropsin solution concentrations from 1 – 100 nM. Despite the small (nM) concentrations of netropsin in solution relative to the ~30-mM concentrations of DNA within individual particles, the netropsin solution concentration is *not depleted* by DNA binding, because the solution volume is more than 10^8-times greater than the volume of the small number of porous particles in the sample.

We also use this method to investigate whether netropsin can exhibit less-selective, lower-affinity interactions with a control sequence that lacks an AT-rich recognition region. By performing experiments at higher netropsin concentrations ranging from 1–50-μM, we quantify a binding interaction that is nearly 4-orders of magnitude weaker than the high-affinity association with AT-rich DNA. In addition to identifying this much weaker affinity, Raman spectroscopy also reveals differences in the netropsin functional groups and DNA bases involved in the high- versus low-affinity association. This experiment not only illustrates the range of interaction strengths that can be investigated with this methodology, it also suggests that caution should be exercised when interpreting solution-phase measurements made at concentrations that are orders-of-magnitude greater than the K_d of the interaction.

EXPERIMENTAL SECTION

Reagents and materials. Spherical chromatographic silica particles were purchased from YMC America (Devens, MA) with an average particle diameter of 5-um, a pore diameter of 31-nm (plenty of room to accommodate the ~3-nm hairpin DNA), and a specific surface area of 117 m^2/g, as specified by the manufacturer. The 2,2-dimethoxy-a-thia-2-silacyclopentane used for silica surface modification with thiol groups was purchased from Gelest (Morrisville, PA). Samples of DNA conjugated with disulfide groups prepared by solid-phase synthesis by the University of Utah HSC Care DNA Synthesis Facility, using a 5'-hexyl disulfide-phosphoramidite modifier (C6 SS) from Glen Research (Maravai LifeSciences, San Diego, CA). The DNA sequence used in these experiments were 4 different 23-base hairpin sequences: (C6 SS)-5'-CCC CGA ATT CGT CTC CGA ATT CG-3', (C6 SS)-5'-CCC CGA AAA CGT CTC CGT TTT CG-3', (C6 SS)-5'-CCC CGA TAT CGT CTC CGA TAT CG-3' and (C6 SS)-5'-CCC CGT CAG GTT CTC ACC TGA CG-3'.

Water used in experiments was filtered with a Barnstead GenPure UV water purification system (ThermoFisher, Waltham, MA) and had a minimum resistivity of 18.0 MΩcm. 1,11-bismaleimido-triethylene glycol, ethylenediaminetetraacetic acid (EDTA), sodium chloride, dithiothreitol (DTT), sodium azide, tris(2-carboxyethyl)phosphine hydrochloride (TCEP), netropsin dihydrochloride from *Streptomyces netropsis* were purchased from Sigma-Aldrich (St. Louis, MO); triethylamine from TCI (Tokyo), dimethylformamide (DMF), dichloromethane (DCM), hydrogen peroxide, sodium hydroxide, hydrochloric acid, and sodium phosphate dibasic heptahydrate (Na_2HPO_4 $7H_2O$) were purchased from Fisher Scientific. 2-amino-2-(hydroxymethyl)propane-1,3-diol was purchased from Goldbio (St. Louis, MO).

Thiol functionalization of silica. Functionalization of porous silica particles with thiol groups has been previously described.[24] Briefly, a 20-mg sample of silica particles was washed with a solution of acid piranha (caution: corrosive, strong oxidizer, can react explosively with organics) to remove physisorbed carbon compounds. The particles were then rinsed twice with deionized water and ethanol, and five-times in anhydrous DCM. Particle samples were suspended in DCM and reacted with 2,2-dimethoxy-1-thia-2-silcyclopentane for 1 hour. Excess silane reagent was quenched with ethanol and the sample was washed in ethanol and deionized water. Particles were stored in deionized water at 2°C and were stable for months.

Coupling thiol-DNA to the thiolated silica surface. Samples of 5'-disulfide-conjugated DNA prepared by the University of Utah DNA and Peptide Core Facility. As described in detail elsewhere,[24] the disulfide was reduced in a solution of 50-mM DTT, 1-mM EDTA, and 2% trimethylamine, and the DNA was purified by precipitation by the addition of ethanol, followed

by centrifugation and ethanol washing to remove excess DTT. The thiol-DNA was reacted with a >10-fold molar excess of 1,11-bismaleimido-triethylene glycol in 50/50 DMF/Tris buffer pH 7.4 with 200-mM NaCl and 500-uM TCEP. Following reaction, the maleimide-conjugated DNA was purified by precipitation by addition of ethanol (-20 C), the precipitate was centrifuged and washed with ethanol, DMF, and ethanol. Ethanol was removed by evaporation, and the maleimide-conjugated DNA was rehydrated with aqueous 400-mM NaCl, immediately diluted with an equal volume of DMF, and allowed to react with thiol-functionalized silica particles for 12-hours.

Confocal Raman microscopy. The confocal Raman microscope has been described,[25] and its configuration is as follows. A 647.1 nm excitation beam from a Kr^+ laser (Innova 90, Coherent Int., Santa Clara, CA) was propagated though a bandpass filter and passed through a x4 beam expander (50- 25-4x-647, Special Optics Inc., Wharton, NJ) and reflected off a dichroic beam splitter, and directed into a 1.4-NA, 100x oil-immersion objective (CFL PLAN APO, Nikon Inc., El Segundo, CA), producing a focus with a ~600 nm diameter beam waist. Scattered light from the confocal probe volume was collected by the same objective, transmitted though the dichroic beam splitter, passed thought a long pass filter, and finally focused though the 50-μm slit of a 500-mm focal-length spectrograph (Bruker 500IS) with a 300-line/mm diffraction grating blazed at 762 nm. Light diffracted by the grating was focused onto a charged coupled device detector (iDus 401A, Andor USA, South Windsor, CT).

Well cells for confocal Raman microscopy were constructed by adhering a ~12 mm length of 10-mm i.d., 13-mm o.d. Pyrex glass tubing to a No. 1 glass coverslip using Devcon 5 min epoxy (ITW Devcon, Danvers, MA). To collect spectra, the beam was focused at the solution/coverslip interface and adjusted upward in the z-dimension until particles were in the field of view. The stage was then adjusted in the x and y dimensions until the focus and confocal probe volume were centered in a single porous silica particle. All spectra reported in this work represent the average of 2-minute integrations collected from 6 different particles. The collected spectra were truncated to the frequency region of interest and baseline corrected with a rolling-circle algorithm.[26] Data analysis was carried out in Matlab (Mathworks, Natick, MA) using custom scripts. For quantitative comparisons, Raman spectra of surface-immobilized DNA-hairpin were normalized to the 1094 cm^{-1} phosphate stretching mode, whose intensity is insensitive to base content.[12] While the particle-to-particle reproducibility of unnormalized Raman scattering intensity is excellent (relative standard deviation of 4%), normalization of the spectral intensity to the 1094 cm^{-1} phosphate mode drops the relative standard deviation of the DNA scattering intensity to 0.6%; see Supporting Information (Figures S1-S2).

RESULTS AND DISCUSSION

Surface immobilization of DNA hairpins to porous silica. To immobilize DNA hairpin sequences we use a bismaleimide reagent to cross-link thiol-functionalized DNA to porous silica surfaces derivatized with thiol functional groups.[24] By first reacting thiol-DNA with a large molar excess of the bismaleimide, the primary Michael-addition reaction product is DNA conjugated to a maleimide functional group through a thiosuccinimide bond. Following a purification step, a second Michael addition is performed by reacting the maleimide-DNA conjugate with thiolated porous silica particles (details in Experimental Section). Due to the efficiency of the Michael addition reaction, the resulting DNA surfaces densities from this protocol are nearly a full monolayer, ~400 nmol/m^2,[24] producing within-particle concentrations of the immobilized 23-mer DNA that are sufficiently high (~30 mM) to be detected with confocal Raman microscopy.

To verify immobilization of the 23-mer DNA hairpin, thiol-functionalized silica particles were characterized prior to and following reaction with the maleimide-DNA conjugate with confocal Raman microscopy. The Raman spectrum of thiol-functionalized silica shows SiO_2 stretching modes (750 – 1000 cm^{-1}), a water bend (1650 cm^{-1}), along with C-C and CH_2 stretching modes (1025 – 1500 cm^{-1}); see Figure 1. Thiol-functionalized particles reacted with the maleimide-DNA conjugate show Raman scattering from both DNA and the cross-linking reagent (Figure 1). Specific nucleoside and backbone phosphate modes are labeled accordingly. Additionally, the distinctive thiosuccinimide stretch (1780 cm^{-1}) associated with the thiol-reactive bismaleimide cross-linker is consistent with DNA immobilization by the conjugate chemistry described above.

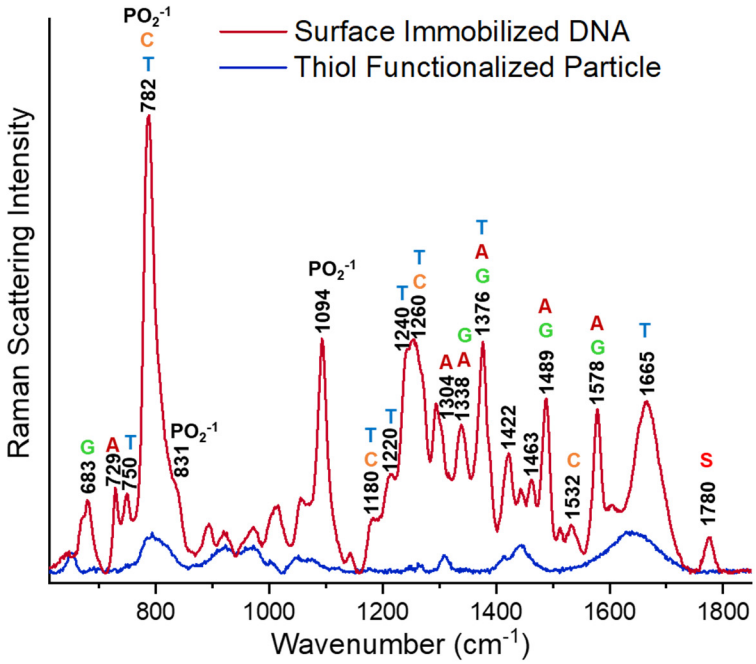

Figure 1. Immobilization of thiol-functionalized DNA to thiolated silica by sequential Michael-addition reactions with a bismaleimide linker. Thiol-functionalized silica particle before (blue) and after (red) reaction with maleimide conjugated DNA. Raman scattering bands from DNA bases and phosphate modes are labeled, and **S** indicates the succinimide stretch from thiol-reacted bismaleimide linker.

Sensitivity of Raman spectroscopy to DNA base content and primary sequence. Raman spectroscopy has previously been used to study the base-content, sequence, and structure

of DNA in free solution.[12-19] To investigate the capability of Raman spectroscopy measurements to characterize surface-immobilized DNA, we examine changes in the Raman spectra arising from differences in base content and sequence of 4 different DNA hairpins. Using the above protocol, the following 23-mer hairpin sequences were immobilized on porous silica surfaces: 5'-CCC CGA ATT CGT CTC CGA ATT CG-3' (designated AATT), 5'-CCC CGA AAA CGT CTC CGT TTT CG-3' (designated AAAA), 5'-CCC CGA TAT CGT CTC CGT ATA CG-3' (designated ATAT)and a control sequence lacking repeated A/T base pairing: 5'-CCC CGT CAG GTT CTC ACC TGA CG-3' (designated Control). It should be noted that three of these sequences have equivalent base content and only differ in the sequence of the adenine- and thymine-rich recognition region.

Using confocal Raman microscopy, the four samples of particles, each with a different hairpin sequence, were examined, and their Raman spectra are compared in Figure 2. Because the number of bases in the four surface-immobilized hairpins are the same, spectra can be normalized to the scattering intensity of the phosphate stretch (1094 cm^{-1}), which is insensitive to base composition,[12] so that differences in the scattering from the DNA bases arising from differences in base content and sequence can be assessed on an equal-molar basis.[12, 20] The ATAT/TATA-containing hairpin sequence and the control sequence show distinct differences in the A-T and G-C base content, where characteristic guanine (685, 1316 and 1491 cm^{-1}) and cytosine (780 and 1528 cm^{-1}) bands exhibit negative intensities and adenine (730, 1340 and 1375 cm^{-1}) and thymine (753, 1375 1674 cm^{-1}) bands show positive intensities in the difference spectrum.

In addition to resolving differences in base-content, literature reports suggest that so-called adenine tracks (or A-tracks) can affect the structural polymorphism of DNA by modulating the stacking and orientation of adenine and thymine nucleotides.[27-29] Previous solution Raman spectroscopy measurements resolved different melting behaviors and spectral characteristics, related to adenine, thymine and sugar-phosphate coupled stretching modes, arising from unique folding of Poly(dA)-Poly(dT) and Poly(dA·dT)-Poly(dA·dT) duplex sequences.[16, 17] To date, the only *in-situ* optical technique capable of discerning differences in surface-immobilized DNA primary sequences is chiral sum-frequency vibrational spectroscopy.[30]

To determine whether interfacial Raman spectroscopy measurements are capable of distinguishing DNA hairpins of equivalent base content that differ in their respective primary sequences, the spectra of three sequences were compared. We first compare the two sequences that were anticipated to have the most significant difference: the constant A·T (AAAA/TTTT)

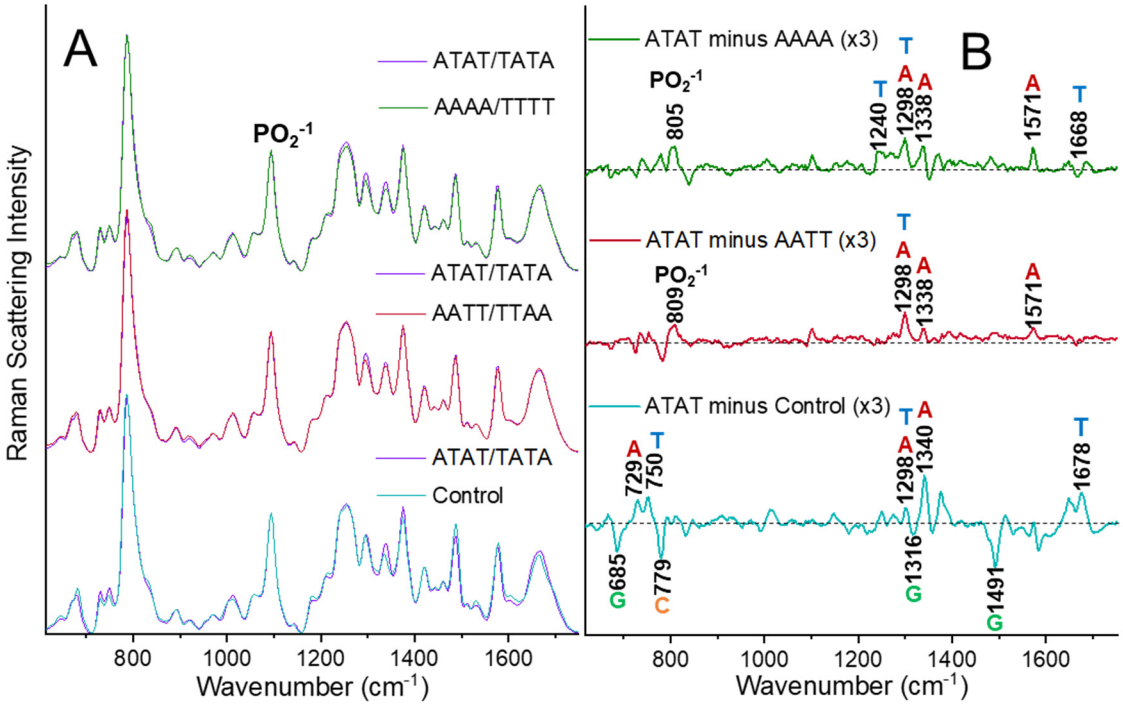

Figure 2. Raman spectra of four surface-immobilized 23-mer hairpin sequences. (A) Spectra from ATAT/TATA (purple), AATT/TTAA (red), AAAA/TTTT (green) and control sequences (cyan), all normalized to the 1094 cm^{-1} phosphate stretch. (B) Difference spectra: ATAT/TATA – AAAA/TTTT (green), ATAT/TATA – AATT/TTAA (red), and ATAT/TATA – control (cyan).

duplex and alternating duplexes A·T/T·A (ATAT/TATA). The ATAT/TATA – AAAA/TTTT difference spectrum reveals subtle differences, where changes in the intensity of the 840 cm^{-1} phosphodiester C5'–O5'–P–O3'–C3' stretch were observed. The greater intensity of this phosphate mode in the A-track sequence is consistent with previous solution-phase Raman measurements and was attributed to ordering of the backbone phosphate.[16] Additional features include the intensity contributed by the thymine stretching modes 1648, 1665 and 1685 cm^{-1} which are coupled to the C4=O, C5=C6 and C2=O stretching modes, respectively[16, 31, 32] (see structures of the DNA bases in Supporting Information, Figure S3). In addition, we detect greater intensity of the 1665 cm^{-1} thymine scattering of the alternating A·T/T·A duplex sequence relative to the 1648 and 1685 cm^{-1} modes of the constant A·T track sequence; these spectral signatures are all consistent with prior work distinguishing these sequences.[16, 32] We also find a series of changes in the intensities of other adenine- and thymine-stretching modes that have not been previously reported: 1298, 1337, 1487, 1571, 1554 cm^{-1}.

In addition to the comparison of the purely alternating A·T/T·A and constant A·T track duplex sequences, we also compare a sequence containing a combination of both. Comparison of the ATAT/TATA and AATT/TTAA duplexes reveals fewer differences, and the magnitudes of the peaks in the difference spectrum are less intense. The smaller difference in the intensities of

these bands is consistent with the AATT/TTAA duplex comprising a combination of base stacking resulting in a spectrum that is more similar to the ATAT/TATA duplex than the AAAA/TTTT duplex. Collectively, these results show the structural sensitivity of Raman spectroscopy since it can reveal differences in base content of immobilized DNA while also being sensitive to the DNA sequence.

Sequence selectivity of netropsin binding to surface-immobilized DNA hairpins. Netropsin is an antimicrobial poly-pyrrole peptide that was originally isolated from the bacterium *Streptomyces netropsis*.[33] Netropsin was among the first small molecules discovered to display high levels of selectivity towards AT-rich sequences of duplex-DNA. Based on studies of selectivity,[23, 34] energetics,[21] and structure,[35-39] netropsin has been shown to associate with high affinity to the minor groove of AT-rich sequences though the coordination of hydrogen bonds with the C2 carbonyl of thymine and N3 nitrogen of adenine, where the amide groups of netropsin act as hydrogen bond donors.[39] The inability for netropsin to associate with GC-rich duplex sequences has been thought to arise from the presence of the amine at the C2 position of guanine, where due to its protrusion from the minor groove, it creates a steric barrier to binding.[21, 35, 39]

For a methodology to be useful in measuring association of small-molecules to specific sequences of surface-immobilized duplex-DNA, the interactions must be both detectable and specific to a DNA recognition sequence. Based on the high affinity and selectivity of netropsin association with AT-rich sequences of DNA derived from NMR,[36] x-ray crystallography,[35, 37, 38] and vibrational spectroscopy,[18, 32, 40, 41] the binding of netropsin to AT-rich duplex-DNA was chosen as a system to test the proposed experimental approach. A spectrum of netropsin in free solution was collected to determine the characteristic vibrational modes; additionally, this spectrum serves as a standard to compare the bound forms of netropsin to an unbound conformation. The molecular structure, functional groups, vibrational spectrum, and band frequencies of netropsin in a 4-mM solution at are shown in Figure 3, where N-methylpyrrole groups are noted with orange labels and amide functional groups highlighted in green. Band frequencies and

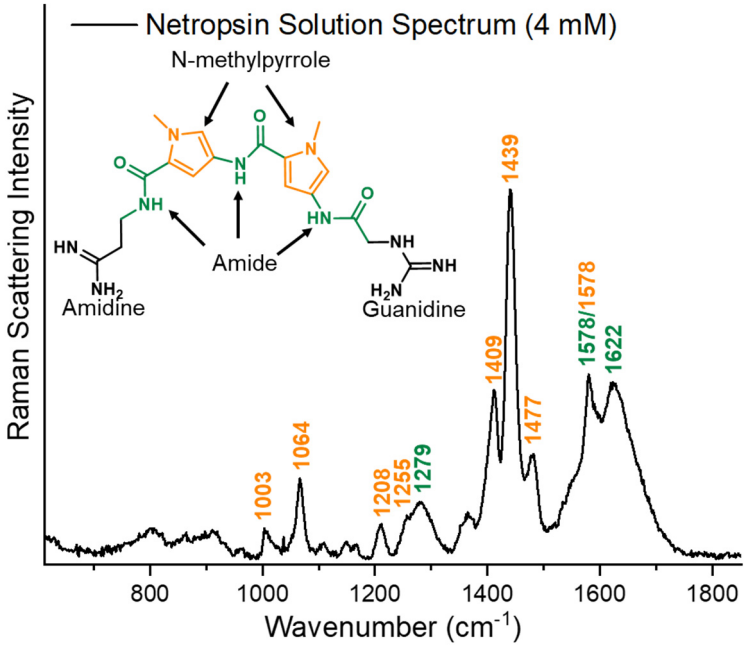

Figure 3. Solution Raman spectrum of netropsin, 4-mM in aqueous buffer. Embedded in the figure is the structure of netropsin along with color-coded band assignments to the N-methylpyrrole and amide functional groups, respectively.

assignments for netropsin in free solution are included in Table S1 (Supporting Information). The detection limit for netropsin is ~150 μM, indicating that netropsin in solution at concentrations below this limit will not contribute to measured scattering in the particles.

To establish whether selective netropsin binding to surface-immobilized DNA hairpin sequences can be detected by Raman microscopy, 100-nM netropsin solutions were prepared and equilibrated with particle samples functionalized with the 4 different hairpin sequences introduced in the previous section. Three of the sequences contain an AT-rich recognition region, where the dissociation constant should be in the range of 3 – 25 nM;[23] one sequence lacking an AT-rich region acts as a control and is anticipated to not form any detectable interactions at 100-nM solution concentrations of netropsin. Raman spectra of each particle sample were acquired prior to and following equilibration with netropsin and are plotted in Figure 4.

In agreement with the expected binding selectivity, there is no detectable change in the Raman spectrum of the control sequence (Figure 4) prior to and following equilibration with 100-nM netropsin. In contrast to the control sequence, there are distinct changes in the spectra of the other three hairpin duplex sequences (AAAA/TTTT, AATT/TTAA and ATAT/TATA) upon equilibration with netropsin. A benefit of using Raman spectroscopy for detecting small-molecule association with immobilized DNA is that the scattering can be assigned to the vibrational modes of specific functional groups. For example, the presence of the netropsin N-methylpyrrole group can be affirmed based on the observation of distinctive 1578, 1064, ~1413 and ~1437 cm^{-1} pyrrole-ring stretching modes.[18, 40, 41] Additionally, netropsin amide functional groups are confirmed by the scattering from the 1530 – 1570 cm^{-1} amide II and ~1638 cm^{-1} amide I stretching modes (see Table S1).[18, 40, 41] These results establish that the binding of netropsin from a 100-nM solution is specific to sequences that include an AT-rich recognition region. The results also demonstrate that detection by Raman spectroscopy can

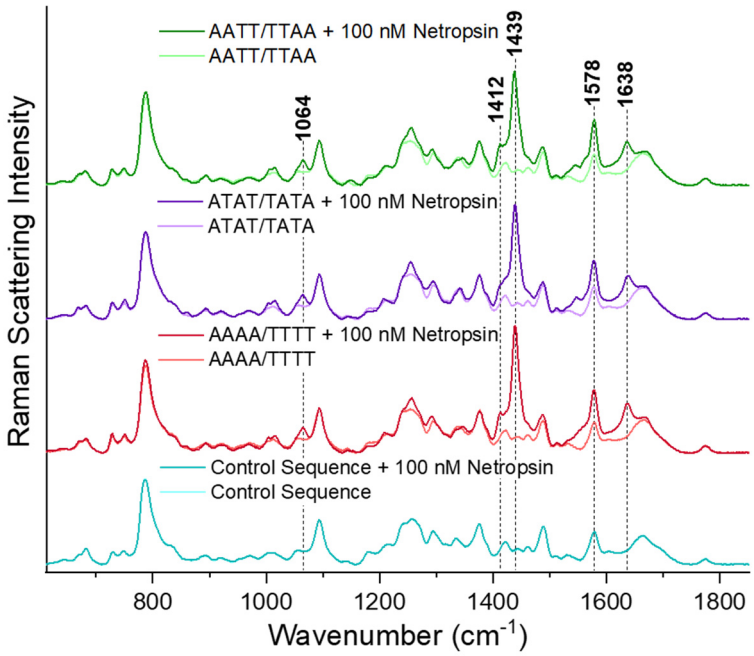

Figure 4. Comparison of netropsin binding to different immobilized hairpin sequences. Each overlaid pair of spectra show the sequence prior to (lighter shade) and following equilibration with 100-nM netropsin (darker shade). Control sequence (cyan), AAAA/TTTT sequence (red), AATT/TTAA sequence (purple), and ATAT/TATA sequence (green).

provide structurally informative evidence of the binding of a small molecule to a DNA sequence based on the scattering of its functional groups.

Netropsin binding isotherms. Having established that high-affinity association of netropsin is specific to sequences that include an AT-rich recognition region, we apply this methodology to determine association constants and to resolve the differences in affinities that depend on the sequence of the DNA duplex. With anticipated dissociation constants in the range of 3 to 25 nM,[21-23] we quantitatively assess the association of netropsin with the three AT-rich sequences by varying the netropsin solution concentration over a range of 1 to 100 nM. To ensure that the solution concentration of netropsin was not depleted at low solution concentrations, samples were prepared with sufficient solution volume to provide a >100-fold molar excess of netropsin compared to the surface-immobilized DNA in the sample.

For each of the particle samples, Raman spectra of six individual particles were acquired, averaged, baseline corrected, normalized to the 1094 cm^{-1} phosphate stretch, and plotted. The results in Figures 5 – 7 show the netropsin concentration-dependent Raman spectra for each hairpin sequence in the spectral region dominated by netropsin scattering; spectra covering the full frequency range are provided in Supporting Information (Figures S4-S7). Strong netropsin association is observed for all three sequences, where Raman scattering from netropsin can be detected at the lowest (1-nM) solution concentration. To quantify the accumulation of netropsin, the netropsin scattering contribution was isolated by subtraction of the spectrum of DNA collected in the absence of netropsin. By scaling this isolated netropsin spectrum, the amplitude of the netropsin scattering intensity in each concentration-dependent spectrum could be determined by least squares fitting (see Supporting Information, Figures S8-S12). Binding isotherms were produced by plotting the resulting netropsin amplitude versus the netropsin solution concentration, and the results are included in Figures 5 – 7. Each data set was fit to a Langmuir binding isotherm using non-linear least squares to determine the association constant, K_a, and maximum signal, Γ_{max}.

The dissociation constant K_d ($=1/K_a$) determined from each fit is listed in each figure, where the reported uncertainty is twice the standard error of the fit, which was found to be equivalent to the measurement reproducibility determined from replicates. Using this method, the K_d of netropsin binding to the AATT/TTAA, AAAA/TTTT and ATAT/TATA recognition duplexes were found to be 4.6 ± 0.8 nM, 5 ± 1 nM, and 16 ± 6 nM, respectively. The affinity of netropsin binding to the AATT/TTAA sequence has been previously investigated by isothermal calorimetry and surface-plasmon resonance,[21, 23] and the dissociation determined in the present

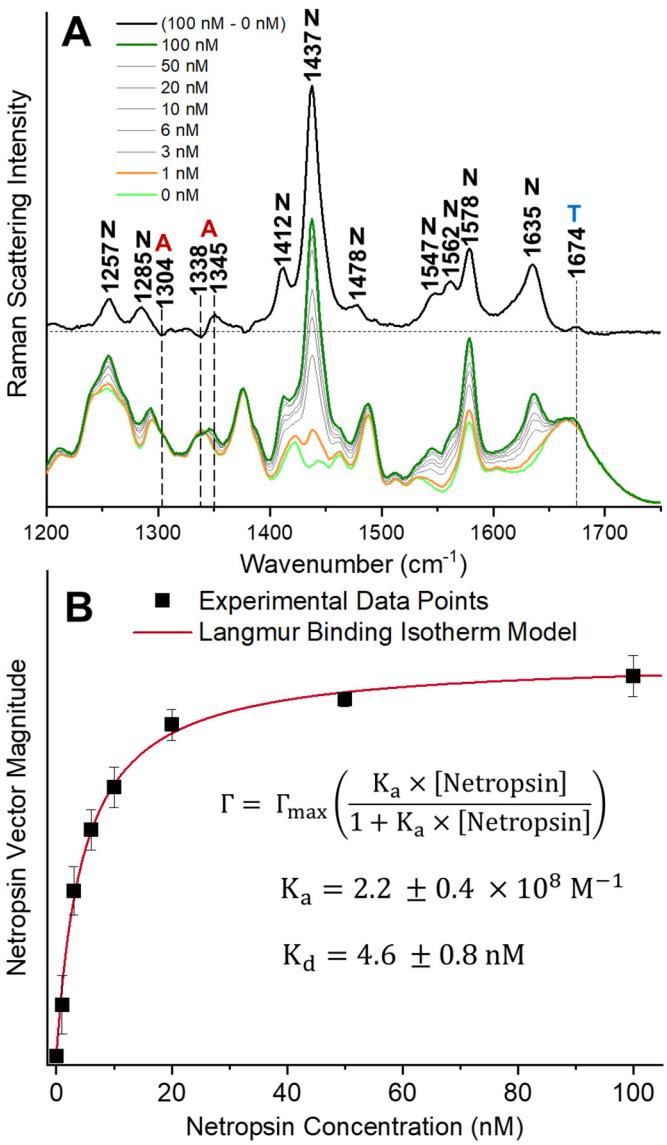

Figure 5. A) Concentration-dependent binding of netropsin (0-100 nM) to the AATT/TTAA sequence, with 100-nM difference spectrum at the top. B) Netropsin magnitude versus netropsin solution concentration, fit to a Langmuir isotherm.

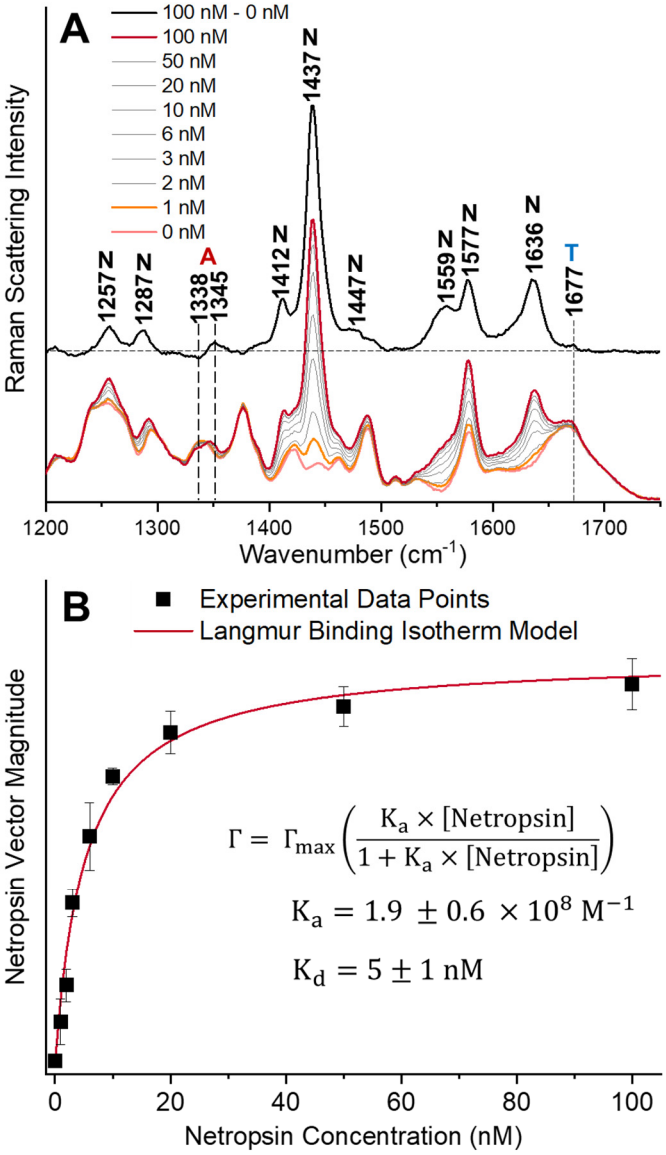

Figure 6. A) Concentration-dependent binding of netropsin (0-100 nM) to the AAAA/TTTT sequence, with 100-nM difference spectrum at the top. B) Netropsin magnitude versus netropsin solution concentration, fit to a Langmuir isotherm.

work was in agreement with these previous results (comparisons are in Supporting Information, Table S2). Our results show that netropsin associations with the AATT/TTAA and AAAA/TTTT duplexes are equivalent in strength, whereas our measurements reveal a lower affinity of netropsin binding to the ATAT/TATA duplex sequence.

The enrichment of the netropsin concentration within the particle relative to the solution can be estimated from these results. The surface coverage of DNA for these particles is 4.6 x 10^{-7} mol/m^2, determined from the scattering intensity of the succinimide stretching mode at 1780 cm^{-1} (see Figure 1) relative to a silica immobilized phenyl-maleimide standard whose surface coverage was found by elemental carbon analysis.[24] By multiplying the DNA surface coverage by the specific surface area of the porous silica (117 m^2/g) and the silica particle density (0.67 g/mL) the within particle concentration of DNA was found to be 36 mM. From the isotherms, we have clear evidence that netropsin concentration saturates according to a Langmuir response. Based on this observation and assuming that saturation corresponds to each DNA hairpin binding one netropsin molecule, then at a solution concentration equal to Kd, half of the DNA hairpins are occupied. The concentration enrichment of netropsin within the particle relative to solution is then given by half the internal concentration of DNA in the particle divided by Kd. For the AATT sequence, for example, the enrichment is 18 mM/4.6 nM = 3.9 x 10^6, which requires that the solution volume be >10^7 greater than the volume of particles in the sample to avoid depleting the solution concentration.

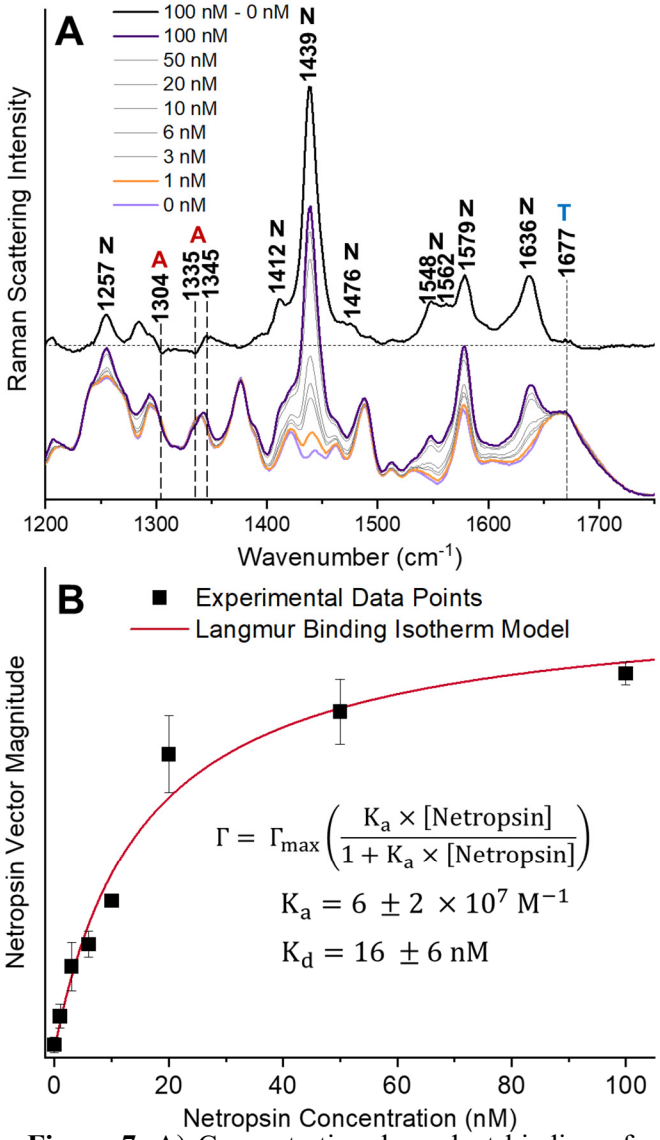

Figure 7. A) Concentration-dependent binding of netropsin (0-100 nM) to the ATAT/TATA sequence, with 100-nM difference spectrum at the top. B) Netropsin magnitude versus netropsin solution concentration, fit to a Langmuir isotherm.

Along with reporting the affinities of netropsin binding the specific AT-rich DNA sequences, the Raman spectra also reveal base-specific vibrational modes that shift as a function of netropsin association. For example, for all recognition sequences, the binding of netropsin was correlated with an increase in the intensity of the 725 cm^{-1} adenine stretch and its shift to 729 cm^{-1}. While the 750 cm^{-1} thymine ring stretch was observed to shift to 753 cm^{-1} and increase in intensity for the AAAA/TTTT and ATAT/TATA duplexes, this band was observed to simply broaden to

lower frequencies in the case of the AATT/TTAA recognition region (see high resolution difference spectra in Supporting Information Figures S13-S15).

In addition to changes in adenine and thymine ring-stretching modes, the functional groups involved in the association interaction can also be identified from changes in other vibrational modes in these spectra. Specifically, it is understood that netropsin acts as a hydrogen bond donor with N3 nitrogen of adenine and C2 carbonyl of thymine in the minor groove.[42] Using previously published assignments based on DFT calculations,[43-45] the following vibrational modes are identified and discussed. In the case of adenine, the 1304 cm^{-1} (in plane ring stretch, bend: C2-H, C8-H, N9-H, str: C6-N1, C8-N9, N3-C4) shifts to lower frequencies and the 1337 cm^{-1} adenine in-plane stretch (C2-N3, C5-N7, bend N9-H) is observed to shift to 1347 cm^{-1}. Although these vibrational modes involve a combination of intramolecular motions, both shifts are coupled to the N3 nitrogen. Additionally, these changes are consistent with prior FTIR measurements[32] and UV resonance Raman[40] measurements that have reported distortions and band narrowing of these two modes upon polypyrrole peptide binding to DNA.

In addition to adenine, there is also a distinctive decrease in the C2=O carbonyl stretching frequency of thymine from 1685 cm^{-1} to 1674 or 1677 cm^{-1} upon netropsin association. Previous FTIR measurements reported an equivalent shifting of the C2=O stretch to lower frequencies upon netropsin binding.[32] In our work, the 1674 cm^{-1} band is a noticeable feature in the netropsin-bound spectrum in the AATT/TTAA duplex, with slightly weaker intensity at 1677 cm^{-1} for AAAA/TTTT duplex, and weaker still when netropsin is bound to the ATAT/TATA duplex sequence. Previous structural analysis has revealed that netropsin forms fewer hydrogen bonds with thymine when bound to the ATAT/TATA duplex, compared to the AATT/TTAA duplex sequence.[35-38] The difference in the behavior of the C2=O thymine carbonyl band likely relates to differences in the number and/or strength of hydrogen bonds that netropsin forms with a target sequence, which in turn impacts differences in the observed affinity. For example, our results show that netropsin forms the lowest affinity interaction with the ATAT/TATA duplex and the lowest intensity of the C2=O thymine stretch (relative to the higher affinity sequences) may reveal the importance of this particular functional group as it relates to primary sequence selectivity.

Lower selectivity binding of netropsin to an off-target sequence. In addition to the high affinity interactions of netropsin with AT-rich sequences, there is evidence that netropsin may form less specific and weaker interactions with DNA when present at higher (micromolar) solution concentrations.[34] The ability to characterize lower affinity interactions of small molecules with DNA is crucial to distinguish the behavior at high solution concentration regions that may drive less-specific, off-target interactions. Additionally, nearly all structurally-informative spectroscopic

assays that are carried out in free solution for characterizing association interactions require the solution concentrations of DNA in the range of 20 – 60 mg/ml to achieve detection, with correspondingly high (millimolar) concentrations of the small-molecule required to equilibrate with the DNA in the sample.[19, 32, 40, 41] These high concentrations of both DNA and the small-molecule needed for detection in free solution are, in many instances, *up to 6 orders of magnitude greater than the K_d* of a high-affinity interaction that is being investigated. Cases where the small molecule being studied has potentially more than a single binding mode[46] raise the question: does the detectable association with DNA that is measured at high solution concentrations arise purely from a single high-affinity interaction, or does it sample associations that derive from a distribution of affinities?

As shown above, the netropsin associations with AT-rich sequences measured at nanomolar concentrations follow a single binding-site Langmuir isotherm, and from this result, we can confidently assert that that the observed interaction between netropsin and these target sequences arises from a single, high-affinity association. To assess the possibility of lower affinity interactions of netropsin with DNA might occur at much higher netropsin concentrations, particles functionalized with the off-target control sequence (that exhibited no detectable netropsin binding at 100 nM) were dispersed in high concentration solutions (up to 50-μM) of netropsin and characterized with confocal Raman microscopy. Note that non-specific interactions of netropsin with the thiolated-silica surface without immobilized DNA can be observed at high solution concentrations; however, control experiments rule out its influence on surfaces having a full monolayer of immobilized off-target DNA (see Supporting Information, Figures S16-S18).

As shown in Figure 8, there is a clear increase in the intensity of netropsin scattering due to its association with the control sequence from solution concentrations in the micromolar range. The presence of netropsin is verified by the appearance of its characteristic vibrational modes, including the N-methylpyrrole related modes: 1065, 1352, 1410, 1439, 1481 and 1587 cm^{-1} and characteristic 1285 cm^{-1} amide III, 1580 cm^{-1} amide II and 1640 cm^{-1} amide I (Table S1). Compared to the netropsin spectra associated with high-affinity AT-rich sequences, there are clear differences in the band ratios and frequencies of the netropsin amide modes as well as distinct changes in the characteristic of the pyrrole modes, discussed in the next section.

Plotting the bound netropsin scattering intensity against its solution concentration shows a response that can modeled by a Langmuir isotherm. The dissociation constant from the fit of these data was found to be 20 ± 4 μM, 4-orders of magnitude weaker affinity than the high-affinity association with AT-rich sequences. The reported K_d is in the concentration range where less sequence-selective binding of netropsin has been observed with DNA foot printing by cleavage inhibition.[34] To our knowledge, this analysis marks the first observation of different small-molecule binding states to dsDNA informed by structural analysis combined with a measurement of binding affinity with Raman spectroscopy.

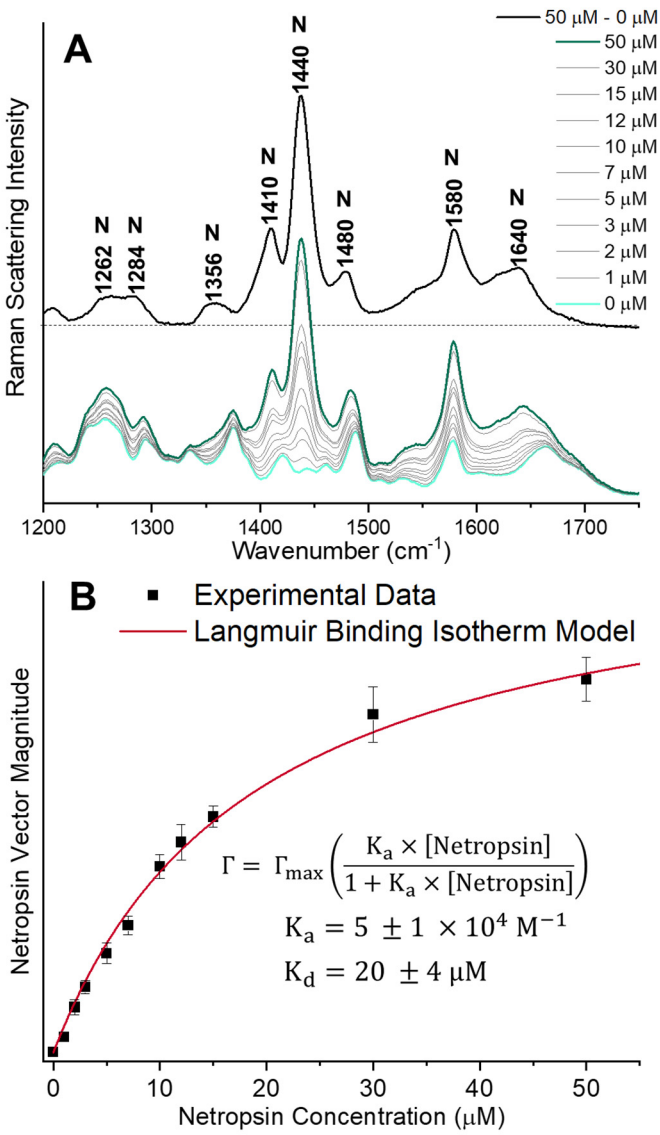

Figure 8. A) Concentration-dependent binding of netropsin (0-50 μM) to the control sequence, with 50-μM difference spectrum at the top. B) Netropsin magnitude versus netropsin solution concentration, fit to a Langmuir isotherm.

Conformational analysis of netropsin. In the previous sections, we have established that netropsin binds at low nanomolar concentrations to AT-rich sequences, while also capable of forming lower affinity, less specific interactions with a control sequence at micromolar solution concentrations. It is clear from the comparison of the resolved netropsin spectra in Figure 9 that each spectrum is unique with respect to band intensities, frequencies, and peak shapes. We first compare the vibrational spectra of the 3-high high affinity recognition regions to the unbound solution netropsin spectrum. Focusing on the amide vibrational modes, the binding to DNA is accompanied with significant band narrowing and shifts in frequency. In all instances, the amide III mode narrows and shifts from 1280 cm^{-1} to ~1286 cm^{-1}, the amide II narrows, and splits from the 1578 cm^{-1} to form a shoulder peak ranging in frequencies 1530 – 1570 cm^{-1} and the amide I mode significantly narrows and shifts from 1622 cm^{-1} to 1636 cm^{-1}. In addition to the changes in the amide modes, there are also significant changes in the relative intensities of the

pyrrole-derived modes. Both the 1409 cm^{-1} and 1477 cm^{-1} pyrrole ring stretching modes decrease in their respective intensities (relative to the predominant 1439 cm^{-1} pyrrole ring stretch) and narrow in their respective bandwidths.

The general observation of band narrowing is consistent with the netropsin adopting a more constrained conformation upon association with the minor groove of DNA. Additionally, the decreases in the intensities of the pyrrole-related modes are likely a consequence of the pyrrole group transitioning from a high dielectric aqueous environment to the minor groove of the DNA, where it is sequestered from water. The significant frequency shifting of the amide vibrational modes is consistent with loss of hydrogen bonding with water molecules and the active involvement of these functional groups in the coordination with DNA.

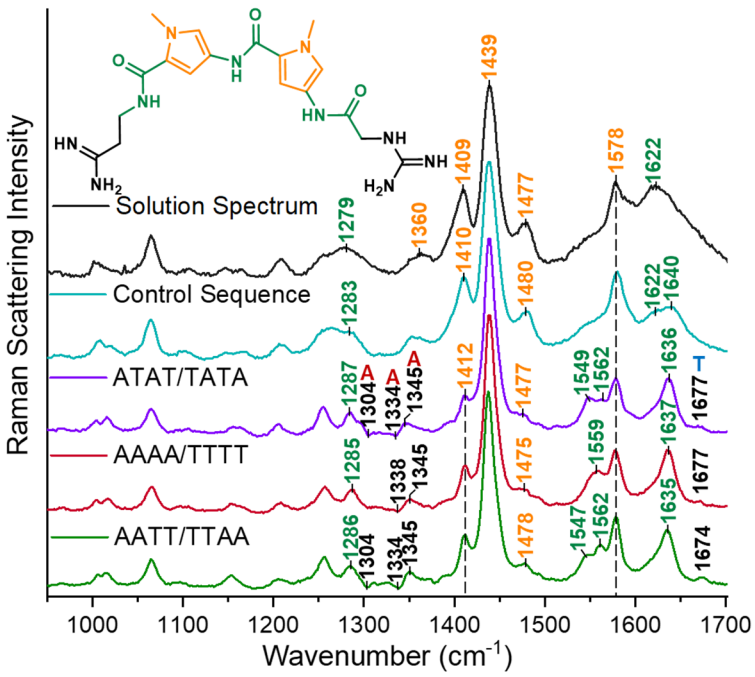

Figure 9. Comparison of resolved netropsin spectra. Top to bottom: netropsin (4 mM) in free solution, netropsin bound to control sequence from 50-μM solution, netropsin bound to the AT-rich sequences from 100-nM solution: ATAT/TATA sequence, AAAA/TTTT sequence, AATT/TTAA sequence.

In addition to the differences between the vibrational spectrum of netropsin between the unbound and high-affinity bound state, there are also discernable differences in the spectra of netropsin bound to the three AT-rich sequences investigated. Specifically, there are clear difference in the ratios of the amide I and II modes along with differences in the resulting peak splitting of the amide II stretch, where the shoulder peak intensity spans 1548 – 1562 cm^{-1}. Previous crystal structure and solution NMR analysis have shown that not only do the number of hydrogen bonds that netropsin forms differ between recognition sequences, but the specific amide functional group coordinating the hydrogen bond differs depending on the sequence of the AT-rich recognition region. The distinct differences in the amide II and I modes observed in the current work are consistent with the amide functional groups forming a series of unique interactions with the AATT/TTAA, ATAT/TATA and AAAA/TTTT duplex sequences.

In comparison to the netropsin bound to the three high affinity AT-rich sequences, the low-affinity netropsin association state exhibits different spectral behavior. Specifically, the pyrrole vibrational modes (1405, 1440 and 1477 cm^{-1}) are nearly equivalent in their respective

bandwidth and ratios to the solution netropsin spectrum. However, there are changes in the peak ratios of the amide II and I vibrational modes along with shifting of the amide III and amide I modes that differ from both the solution spectrum and high-affinity association state. Although subtle, there is a slight distortion of the amide III mode upon association. Additionally, although the 1578 cm^{-1} amide II stretch remains unchanged in its frequency (relative to the solution spectrum), the 1620 cm^{-1} amide I stretch is observed to split by forming a shoulder at 1640 cm^{-1}.

Based on the distortion of the amide III stretch and the splitting of the amide I stretch, we conclude that the low affinity association interaction involves the amide functional group. However, due to the peak remaining broadened, this is consistent with a weaker, less constrained conformation adopted by netropsin. Additionally, in contrast to netropsin bound to the high-affinity sequences, our results suggest that the pyrrole group must largely remain solvated in aqueous solution due to the unchanging features of these bands relative to the spectrum of netropsin in aqueous solution. The less constrained conformations of the amide groups compared to high-affinity binding and the pyrrole remaining in contact aqueous solution are consistent with a 4000-fold weaker affinity determined for netropsin association with the off-target sequence.

Conclusions. In this work, we have developed a new experimental approach to carry out Raman spectroscopic characterization of small-molecule association with surface-immobilized DNA. The methodology takes advantage of high surface area of porous silica supports, which provide readily detectable (~30-mM) local concentrations of the immobilized DNA in the interior of individual particles that can be probed by confocal Raman microscopy. Unlike conventional solution-phase spectroscopic measurements, this approach allows the characterization of association interactions at nanomolar solution concentrations of small-molecules in the range of the dissociation constants for strong binding affinities. The method confirmed the selectivity of netropsin binding to adenine and thymine-rich sequences, whereas no detectable netropsin association was detected at nanomolar concentrations with an off-target control sequence having only isolated AT-base pairing. This measurement was also shown to be capable of producing binding isotherms over a wide range of K_d, from low nanomolar to high micromolar, allowing the determination of netropsin binding affinities to both AT-rich and off-target sequences. Finally, from changes in the vibrational frequencies and intensities of both the immobilized DNA and bound small-molecule target that accompany association, insight can be gained into the nature of the interactions responsible for their interaction.

This work has many potential avenues of application that have yet to be explored. For example, longer and more complex sequences containing multiple recognition regions could be assessed. Additionally, the ability to resolve subtle changes in the vibrational spectra of both the

small molecule and the immobilized DNA upon binding creates an opportunity to gain deeper insight into the structure and interactions responsible for their interaction when combined with DFT calculations. Finally, this work also has to the potential to screen libraries of small molecules for their association with specific sequences of DNA.

ASSOCIATED CONTENT

Supporting Information.

Additional information on the quantitative reproducibility of surface-immobilized DNA, the structure and ring-numbering of DNA bases, netropsin vibrational modes and frequencies, full spectra of concentration-dependent experiments, least-squares analysis of concentration-dependent spectra, high-resolution spectra of adenine and thymine stretching modes, a table of binding affinity results, non-specific adsorption control experiments, and references.

ACKNOWLEDGEMENTS

This work was supported by the National Science Foundation under Grant CHE-1904424. The authors are grateful to W. Mike Hanson of the University of Utah Core DNA Synthesis Facility for contributions to this project.

REFERENCES

1. Latt, S. A.; Stetten, G.; Juergens, L. A.; Willard, H. F.; Scher, C. D., Recent developments in the detection of deoxyribonucleic acid synthesis by 33258 Hoechst fluorescence. *J. Histochem. Cytochem.* **1975,** *23* (7), 493-505.

2. Kapuscinski, J., DAPI: a DNA-Specific Fluorescent Probe. *Biotech. Histochem.* **1995,** *70* (5), 220-233.

3. Di Antonio, M.; Ponjavic, A.; Radzevičius, A.; Ranasinghe, R. T.; Catalano, M.; Zhang, X.; Shen, J.; Needham, L.-M.; Lee, S. F.; Klenerman, D.; Balasubramanian, S., Single-molecule visualization of DNA G-quadruplex formation in live cells. *Nat. Chem.* **2020,** *12* (9), 832-837.

4. Martin, R. M.; Leonhardt, H.; Cardoso, M. C., DNA labeling in living cells. *Cytometry A* **2005,** *67A* (1), 45-52.

5. Gottesfeld, J. M.; Neely, L.; Trauger, J. W.; Baird, E. E.; Dervan, P. B., Regulation of gene expression by small molecules. *Nature* **1997,** *387* (6629), 202-205.

6. Dervan, P.; Doss, R.; Marques, M., Programmable DNA Binding Oligomers for Control of Transcription. *Anti-Cancer Agents Med. Chem.* **2005,** *5* (4), 373-387.

7. Gurova, K., New hopes from old drugs: revisiting DNA-binding small molecules as anticancer agents. *Future Oncol.* **2009,** *5* (10), 1685-1704.

8. Chen, B.-J.; Wu, Y.-L.; Tanaka, Y.; Zhang, W., Small Molecules Targeting c-Myc Oncogene: Promising Anti-Cancer Therapeutics. *Int. J. Biol. Sci.* **2014,** *10* (10), 1084-1096.

9. Cheung-Ong, K.; Giaever, G.; Nislow, C., DNA-Damaging Agents in Cancer Chemotherapy: Serendipity and Chemical Biology. *Chem. Biol.* **2013,** *20* (5), 648-659.

10. Wilson, W. D., Analyzing Biomolecular Interactions. *Science* **2002,** *295* (5562), 2103-2105.

11. Liu, Y.; Kumar, A.; Depauw, S.; Nhili, R.; David-Cordonnier, M.-H.; Lee, M. P.; Ismail, M. A.; Farahat, A. A.; Say, M.; Chackal-Catoen, S.; Batista-Parra, A.; Neidle, S.; Boykin, D. W.; Wilson, W. D., Water-Mediated Binding of Agents that Target the DNA Minor Groove. *J. Am. Chem. Soc.* **2011,** *133* (26), 10171-10183.

12. Duguid, J. G.; Bloomfield, V. A.; Benevides, J. M.; Thomas, G. J., Jr., DNA melting investigated by differential scanning calorimetry and Raman spectroscopy. *Biophys. J.* **1996,** *71* (6), 3350-3360.

13. Miura, T.; Thomas, G. J., Structural Polymorphism of Telomere DNA: Interquadruplex and Duplex-Quadruplex Conversions Probed by Raman Spectroscopy. **1994,** *33* (25), 7848-7856.

14. Pagba, C. V.; Lane, S. M.; Wachsmann-Hogiu, S., Raman and surface-enhanced Raman spectroscopic studies of the 15-mer DNA thrombin-binding aptamer. *J. Raman Spectrosc.* **2010,** *41* (3), 241-247.

15. Palacký, J.; Mojzeš, P.; Kejnovská, I.; Vorlíčková, M., Does Raman spectroscopy recognize different G-quadruplex arrangements? *J. Raman Spectrosc.* **2019,** *51* (2), 301-312.

16. Movileanu, L.; Benevides, J. M.; Thomas, G. J., Temperature dependence of the Raman spectrum of DNA. II. Raman signatures of premelting and melting transitions of poly(dA)·poly(dT) and comparison with poly(dA-dT)·poly(dA-dT). *Biopolymers* **2002,** *63* (3), 181-194.

17. Benevides, J. M.; Overman, S. A.; Thomas, G. J., Raman, polarized Raman and ultraviolet resonance Raman spectroscopy of nucleic acids and their complexes. *J. Raman Spectrosc.* **2005,** *36* (4), 279-299.

18. Martin, J. C.; Wartell, R. M.; O'Shea, D. C., Conformational features of distamycin-DNA and netropsin-DNA complexes by Raman spectroscopy. *Proc. Natl. Acad. Sci. U.S.A.* **1978,** *75* (11), 5483-5487.

19. Benevides, J. M.; Kawakami, J.; Thomas, G. J., Mechanisms of drug-DNA recognition distinguished by Raman spectroscopy. *J. Raman Spectrosc.* **2008,** *39* (11), 1627-1634.

20. Myres, G. J.; Peterson, E. M.; Harris, J. M., Confocal Raman Microscopy Enables Label-Free, Quantitative, and Structurally Informative Detection of DNA Hybridization at Porous Silica Surfaces. *Anal. Chem.* **2021,** *93* (22), 7978-7986.

21. Marky, L. A.; Breslauer, K. J., Origins of netropsin binding affinity and specificity: correlations of thermodynamic and structural data. *Proc. Natl. Acad. Sci. U. S. A.* **1987,** *84* (13), 4359-4363.

22. Rentzeperis, D.; Marky, L. A.; Dwyer, T. J.; Geierstanger, B. H.; Pelton, J. G.; Wemmer, D. E., Interaction of minor groove ligands to an AAATT/AATTT site: correlation of thermodynamic characterization and solution structure. *Biochemistry* **1995,** *34* (9), 2937-2945.

23. Freyer, M. W.; Buscaglia, R.; Nguyen, B.; David Wilson, W.; Lewis, E. A., Binding of netropsin and 4,6-diamidino-2-phenylindole to an A2T2 DNA hairpin: A comparison of biophysical techniques. *Anal. Biochem.* **2006,** *355* (2), 259-266.

24. Myres, G. J.; Harris, J. M., Stable Immobilization of DNA to Silica Surfaces by Sequential Michael-Addition Reactions Developed with Insights from Confocal-Raman Microscopy. *Anal. Chem.* **2022,** *95* (6), 3499-3506.

25. Kitt, J. P.; Harris, J. M., Confocal Raman Microscopy for in Situ Detection of Solid-Phase Extraction of Pyrene into Single C18–Silica Particles. *Anal. Chem.* **2014,** *86* (3), 1719-1725.

26. Brandt, N. N.; Brovko, O. O.; Chikishev, A. Y.; Paraschuk, O. D., Optimization of the Rolling-Circle Filter for Raman Background Subtraction. *Appl. Spectrosc.* **2006,** *60* (3), 288-293.

27. Haran, T. E.; Mohanty, U., The unique structure of A-tracts and intrinsic DNA bending. *Q. Rev. Biophys.* **2009,** *42* (1), 41-81.

28. Koo, H.-S.; Wu, H.-M.; Crothers, D. M., DNA bending at adenine · thymine tracts. *Nature* **1986,** *320* (6062), 501-506.

29. Leroy, J. L.; Charretier, E.; Kochoyan, M.; Gueron, M., Evidence from base-pair kinetics for two types of adenine tract structures in solution: their relation to DNA curvature. *Biochemistry* **1988,** *27* (25), 8894-8898.

30. Stokes, G. Y.; Gibbs-Davis, J. M.; Boman, F. C.; Stepp, B. R.; Condie, A. G.; Nguyen, S. T.; Geiger, F. M., Making "Sense" of DNA. *J. Am. Chem. Soc.* **2007,** *129* (24), 7492-7493.

31. Tsuboi, M.; Kumakura, A.; Aida, M.; Kaneko, M.; Dupuis, M.; Ushizawa, K.; Ueda, T., Raman scattering tensors in thymine molecule from an ab initio MO calculation. *Spectrochim. Acta Part A* **1997,** *53* (3), 409-419.

32. Liquier, J.; McHami, A.; Taillandier, E., FTIR Study of Netropsin Binding to Poly d(A-T) and Poly dA · Poly dT. *J. Biomol. Struct. Dyn.* **1989,** *7* (1), 119-126.

33. Finlay, A. C.; Hochstein, F. A.; Sobin, B. A.; Murphy, F. X., Netropsin, a New Antibiotic Produced by a Streptomyces. *J. Am. Chem. Soc.* **1951,** *73* (1), 341-343.

34. Van Dyke, M. W.; Hertzberg, R. P.; Dervan, P. B., Map of distamycin, netropsin, and actinomycin binding sites on heterogeneous DNA: DNA cleavage-inhibition patterns with methidiumpropyl-EDTA.Fe(II). *Proc. Natl. Acad. Sci. U.S.A.* **1982,** *79* (18), 5470-5474.

35. Kopka, M. L.; Yoon, C.; Goodsell, D.; Pjura, P.; Dickerson, R. E., The molecular origin of DNA-drug specificity in netropsin and distamycin. *Proc. Natl. Acad. Sci. U.S.A.* **1985,** *82* (5), 1376-1380.

36. Patel, D. J.; Shapiro, L., Molecular recognition in noncovalent antitumor agent-DNA complexes: NMR studies of the base and sequence dependent recognition of the DNA minor groove by netropsin. *Biochimie* **1985,** *67* (7), 887-915.

37. Goodsell, D. S.; Kopka, M. L.; Dickerson, R. E., Refinement of Netropsin Bound to DNA: Bias and Feedback in Electron Density Map Interpretation. *Biochemistry* **1995,** *34* (15), 4983-4993.

38. Nunn, C. M.; Garman, E.; Neidle, S., Crystal Structure of the DNA Decamer d(CGCAATTGCG) Complexed with the Minor Groove Binding Drug Netropsin. *Biochemistry* **1997,** *36* (16), 4792-4799.

39. Dervan, P. B., Molecular recognition of DNA by small molecules. *Biorg. Med. Chem.* **2001,** *9* (9), 2215-2235.

40. Grygon, C. A.; Spiro, T. G., Ultraviolet resonance Raman spectroscopy of distamycin complexes with poly(dA)-poly(dT) and poly(dA-dT): role of hydrogen bonding. *Biochemistry* **1989,** *28* (10), 4397-4402.

41. Lu, D. S.; Nonaka, Y.; Tsuboi, M.; Nakamoto, K., Molecular distortion of distamycin on binding to DNA as revealed by Raman spectroscopy. *J. Raman Spectrosc.* **1990,** *21* (5), 321-326.

42. Nguyen, B.; Neidle, S.; Wilson, W. D., A Role for Water Molecules in DNA−Ligand Minor Groove Recognition. *Acc. Chem. Res.* **2009,** *42* (1), 11-21.

43. Madzharova, F.; Heiner, Z.; Gühlke, M.; Kneipp, J., Surface-Enhanced Hyper-Raman Spectra of Adenine, Guanine, Cytosine, Thymine, and Uracil. *J. Phys. Chem. C* **2016,** *120* (28), 15415-15423.

44. Cho, K.-H.; Choo, J.; Joo, S.-W., Tautomerism of thymine on gold and silver nanoparticle surfaces: surface-enhanced Raman scattering and density functional theory calculation study. *J. Mol. Struct.* **2005,** *738* (1), 9-14.

45. Aroca, R.; Bujalski, R., Surface enhanced vibrational spectra of thymine. *Vib. Spectrosc* **1999,** *19* (1), 11-21.

46. Lewis, E. A.; Munde, M.; Wang, S.; Rettig, M.; Le, V.; Machha, V.; Wilson, W. D., Complexity in the binding of minor groove agents: netropsin has two thermodynamically different DNA binding modes at a single site. *Nucleic Acids Res.* **2011,** *39* (22), 9649-9658.

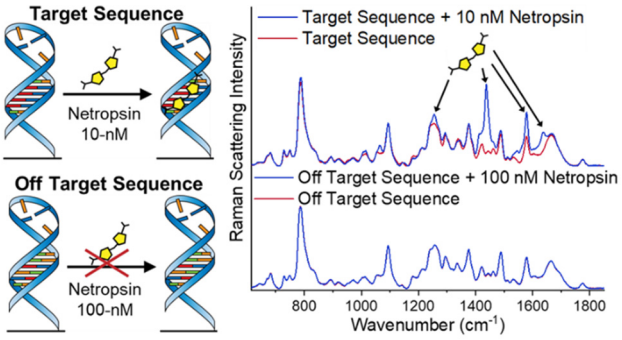
Target Sequence
Netropsin
10-nM
Off Target Sequence
Netropsin
100-nM
Target Sequence + 10 nM Netropsin
Target Sequence
Off Target Sequence + 100 nM Netropsin
Off Target Sequence
Raman Scattering Intensity
800
1000
1200
1400
1600
1800
Wavenumber (cm-1)

TOC GRAPHIC